Disorder unveils Mott quantum criticality behind a first-order transition in the quasi-two-dimensional organic conductor κ-$(ET)_2Cu[N(CN)_2]Cl$

Mizuki Urai,[1] Tetsuya Furukawa,[2] Yasuhide Seki,[1] Kazuya Miyagawa,[1] Takahiko Sasaki,[3] Hiromi Taniguchi,[4] and Kazushi Kanoda[1]

[1]*Department of Applied Physics, University of Tokyo, Tokyo 113-8656, Japan*
[2]*Department of Applied Physics, Tokyo University of Science, Tokyo 125-8585, Japan*
[3]*Institute for Materials Research, Tohoku University, Sendai 980-8577, Japan*
[4]*Department of Physics, Saitama University, Saitama, 338-8570, Japan*

(Received 1 March 2019; revised manuscript received 7 June 2019; published 20 June 2019)

We show the significant impact of weak disorder on the Mott transition by investigating electronic transport in a systematically x-ray-irradiated layered organic conductor under continuous pressure control. The critical end point of the first-order Mott transition is dramatically suppressed by such weak disorder that causes only a minor reduction in the transition temperature of disorder-sensitive nodal superconductivity. Instead, quantum critical scaling of resistance holds at lower temperatures and Fermi-liquid coherence temperature on the metallic side is lowered. Introducing disorder unveils the interaction-induced quantum criticality hidden behind the first-order transition.

DOI: 10.1103/PhysRevB.99.245139

I. INTRODUCTION

The metal-insulator transition (MIT) is one of the central issues in condensed-matter physics. Strong electron-electron Coulomb repulsion drives Bloch waves into spatially localized particlelike states (Mott localization). Randomness in a periodic lattice potential can also cause electron localization due to the interference of electron waves (Anderson localization), which are particularly significant in two dimensions. As such, interaction and disorder localize electrons in different ways. The interplay of the Coulomb interaction and disorder can trigger nontrivial MITs while inheriting the particle-wave duality of electrons. There exist many theoretical investigations on this fundamental issue using various numerical methods [1–12]. To illuminate the interplay in real materials, however, the interaction strength and the degree of disorder need to be precisely and independently varied in a controlled way near the MIT, which has been prohibiting experimental challenges to this issue.

Layered organic conductors with half-filled bands, κ-$(ET)_2X$ [ET = bis(ethylendithio)tetrathiafulvalene and X denotes anion species], are model systems for studying this issue in two dimensions [13]. Among them, κ-$(ET)_2Cu[N(CN)_2]Cl$ (abbreviated κ-Cl hereafter) is best characterized. This material is a Mott insulator with antiferromagnetic ordering below 23 K at ambient pressure [14] and undergoes a first-order transition to a metal, which exhibits superconductivity at 13 K at a hydrostatic pressure of as low as 20–30 MPa. The first-order transition has a critical end point T_{ep} of approximately 40 K [15,16], signifying no symmetry breaking associated with the transition, the same as for the liquid-gas transition. Above T_{ep}, a fan-shaped quantum critical region is extended in the pressure-temperature (P-T) plane [17,18]. Recently, the effect of x-ray irradiation on the structural and electronic properties of a series of κ-$(ET)_2X$ was investigated [19]. Infrared spectroscopy indicates that irradiation induces disorder in the chemical bonds in the anion layers [20], which is suggested to generate random potential modulation in the conducting ET layers by first-principles calculations [21]. Indeed, a remarkable impact of x-ray irradiation is observed on the low-temperature resistivity in κ-Cl at ambient pressure [19]. As the amount of disorder can be regulated by the irradiation time, the evolution of the Mott transition profile in κ-Cl with the x-ray irradiation time illustrates the interplay between interactions and disorder in electron localizations.

In the present work, we investigated the electric transport of the Mott transition system with controlled disorder by measuring the in-plane resistance of a successively x-ray irradiated κ-Cl crystal under temperature and pressure variations using a helium-gas pressure system, which allows for continuous pressure control even at low temperatures (see also the Supplemental Material [22]). We report our finding that the critical end point of the first-order Mott transition is drastically suppressed in temperature by disorder and instead metal-insulator quantum critical fluctuations prevail.

II. EXPERIMENTAL METHODS

The single crystal of κ-Cl used in the present study was $0.3 \times 0.2 \times 0.02$ mm^3 in size. An identical crystal was successively irradiated by white x rays with a nonfiltered tungsten target (40 kV, 20 mA) at room temperature. The corresponding dose rate was approximately 0.5 MGy/h [19,20]. We used a 20-μm-thick crystal, which is far thinner than the x-ray attenuation length of 1 mm or less, to attain homogeneous x-ray-induced disorder over the sample volume. The electrical resistance at irradiation times of 0, 50, 70, and 90 h was measured using the standard dc four-probe method under an isothermal pressure sweep and isobaric temperature sweep using helium gas as the pressure medium. The P-T range

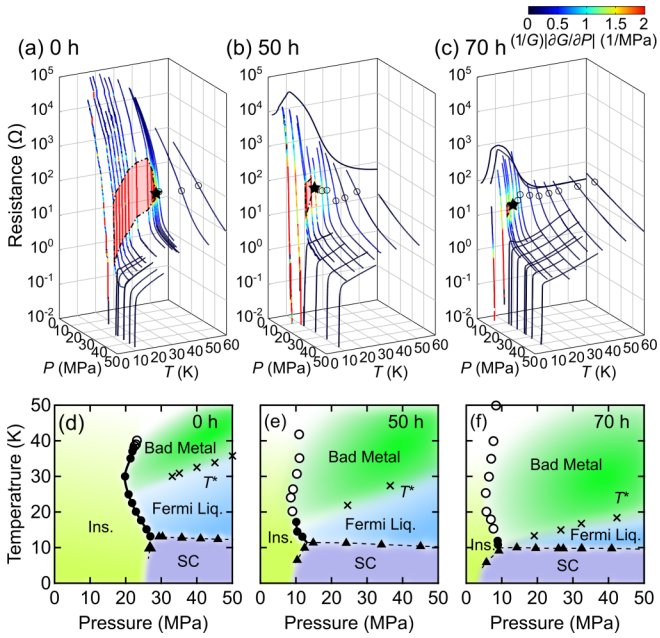

FIG. 1. (a)–(c) Resistance in the P-T planes. The range of color indicates the compressibility of the conductance $|(1/G)\partial G/\partial P|$, and the open circles represent the crossover points corresponding to maxima in $|(1/G)\partial G/\partial P|$. The solid star corresponds to T_{ep}. (d)–(f) Phase diagrams. "Ins.," "Fermi Liq.," and "SC" represent insulator, Fermi liquid, and superconductivity, respectively. The solid and open circles represent points at which major resistance jumps (first-order transitions) and the crossover points appear, respectively. The solid triangles and crosses are the superconducting transition temperatures T_{SC} and the coherence temperatures T^*, respectively (see also the Supplemental Material [22]). We took the set of T^* for $t_{irr} = 0$ h from Ref. [16].

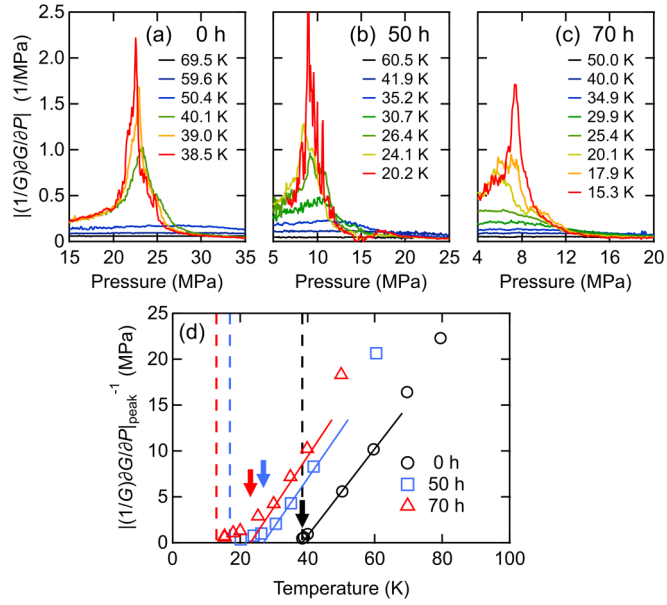

FIG. 2. (a)–(c) Pressure dependence of $|(1/G)\partial G/\partial P|$ at fixed temperatures. The curve at 15.3 K in (c) was determined under a perpendicular magnetic field of 9 T, which was applied to suppress the possible superconducting fluctuations (see also the Supplemental Material [22]). (d) Temperature dependence of the inverse of the peak value in $|(1/G)\partial G/\partial P|$. The solid lines are guides for the eye. The dashed lines and thick arrows indicate T_{ep} and T^*_{ep}, respectively, for each irradiation time.

studied here was limited to the region in which the helium pressure medium was not solidified.

III. RESULTS AND DISCUSSION

The resistance profiles of κ-Cl in the pressure-temperature plane at different irradiation times t_{irr} are shown in Figs. 1(a)–1(c), which trace resistance under an isothermal pressure sweep and isobaric temperature sweep. The result from the pristine sample [Fig. 1(a)] is in agreement with a previous report [15]; the resistance of the pristine sample shows an insulating behavior at low pressure, whereas it shows a metallic behavior at high pressure, with the two regimes separated by the first-order transition, which is characterized by a discontinuous jump in resistance below a critical end point $T_{ep} \sim 38.5$ K. Above T_{ep}, the resistance varies continuously under a pressure sweep. As seen in Figs. 1(b) and 1(c), successive x-ray irradiation progressively reduces T_{ep}, making the insulating behavior at low pressures less prominent. These results demonstrate that the crossover region is extended down to lower temperatures with increased irradiation. This feature is qualitatively reproduced by a very recent report [23]. Decreases in resistance below 10–12 K at low pressures in Figs. 1(b) and 1(c) are ascribed to tiny traces of superconductivity in the bulk insulating phase, which have often been observed [24,25]. The critical end point T_{ep} at which the discontinuous jump in resistance disappears is determined to be 17–20 K for $t_{irr} = 50$ h and 12–13 K for $t_{irr} = 70$ h. As discussed later, this rapid suppression of T_{ep} indicates a surprisingly fragile feature of the first-order transition to disorder. The phase diagrams for $t_{irr} = 0$, 50, and 70 h are shown in Figs. 1(d)–1(f). In addition to the drastic change of the Mott transition profile, the transition boundary shifts slightly negative by 15 MPa, equivalent to changes in lattice constants by 0.03%–0.04% [26]; it should be considered a minor effect of disorder separate from its major effect on the Mott criticality.

To further evaluate the temperature-pressure profile for conductance around the critical end point, we investigate the logarithmic pressure derivative of the isothermal conductance $|(1/G)\partial G/\partial P|$, a sort of "compressibility" of conductance, which forms a peak upon crossing the Widom line of the Mott transition [Figs. 2(a)–2(c)]. Before irradiation, the peak grows progressively when $T_{ep} \sim 38.5$ K is approached from above T_{ep} [Fig. 2(a)], reproducing previous results [15]. Even after irradiation for 50 and 70 h, a similar behavior is observed above the reduced T_{ep} [Figs. 2(b) and 2(c)]. The inverse of the peak value $|(1/G)\partial G/\partial P|^{-1}_{peak}$ is plotted against temperature in Fig. 2(d). Before irradiation, $|(1/G)\partial G/\partial P|^{-1}_{peak}$ is proportional to $|T - T_{ep}|$ for $T \lesssim 60$ K. After irradiation, $|(1/G)\partial G/\partial P|^{-1}_{peak}$ also decreases linearly with temperature down to 35 and 30 K for $t_{irr} = 50$ and 70 h, respectively, and nonlinearly approaches T_{ep}, which is indicated by the dashed lines in Fig. 2(d). The nonlinear decrease in $|(1/G)\partial G/\partial P|^{-1}_{peak}$ may be a manifestation of electronic inhomogeneity or the Griffiths phase (discussed later). The

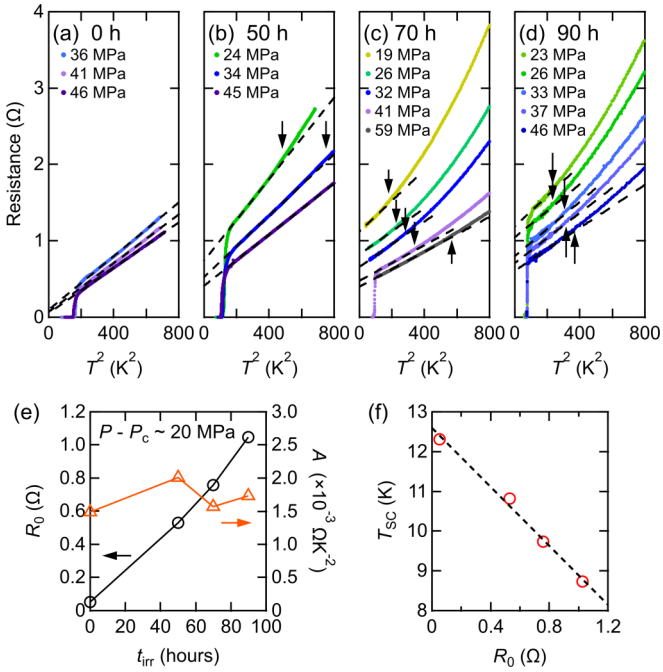

FIG. 3. (a)–(d) Temperature dependence of the resistance. The arrows indicate T^*. (e) Residual resistance R_0 and coefficient A against the irradiation time. The values of R_0 and A plotted here are those at $P - P_c \sim 20$ MPa (see also the Supplemental Material [22]). (f) Plot of T_{SC} versus R_0 at $P - P_c \sim 20$ MPa.

interception of the high-temperature linearity at the horizontal axis denoted by T^*_{ep} [Fig. 2(d)] can be regarded as the nominal critical end point extrapolated from the high-temperature behavior.

Figures 3(a)–3(d) show the resistance versus T^2 at low temperature in the metallic phase. Before irradiation, the Fermi-liquid behavior of $R = R_0 + AT^2$ persists up to above 25 K for each pressure. For $t_{irr} = 50$ h, resistance shows an upward deviation from the T^2 dependence at T^* [indicated in Fig. 3(b)], which decreases as the critical pressure P_c is approached. For $t_{irr} = 70$ and 90 h, the Fermi-liquid region is quite limited to low temperatures close to the superconducting transition temperature T_{SC}, in particular, near P_c. We determined T^* under a magnetic field of 9 T for $t_{irr} = 70$ h, which suppresses the superconductivity [Fig. 3(c)], at 19, 26, 32, and 56 MPa. Thus, the energy scale of the Fermi liquid characterized by T^* remarkably drops off with increasing disorder or approaching the critical pressure P_c. Note that the residual resistance R_0 increases approximately in proportion with the irradiation time [Fig. 3(e)], showing that t_{irr} is a good measure of the intensity of disorder. The absolute value of the in-plane resistivity inevitably has an ambiguity of a factor of several times because of the difficulty in measuring it for a blocklike crystal with an extremely large resistivity anisotropy on the order of 10^4 or more. The residual resistivity $\rho_{\|0}$ determined for five crystals was in the range of 3–12 $\mu\Omega$ cm for $t_{irr} = 0$ h, 30–120 $\mu\Omega$ cm for $t_{irr} = 50$ h, and 60–240 $\mu\Omega$ cm for $t_{irr} = 90$ h. These values are more than one order of magnitude smaller than the Mott-Ioffe-Regel limit, 4 mΩ cm, which is given by Dh/e^2, where $D = 1.5$ nm is the interlayer spacing, h is the Planck constant, and e is the elementary charge. This estimate indicates that the present system is in a weakly disordered regime. The coefficient A, which is supposed to be proportional to the square of the effective mass in the conventional Fermi-liquid theory, does not significantly vary with x-ray irradiation [Fig. 3(e)]. The contrasting behaviors of R_0 and A against t_{irr} are consistent with Matthiessen's rule in the Fermi-liquid regime, in which disorder causes only single-particle impurity scatterings. The remarkable suppression of T^* with increasing disorder, however, is unexplainable by single-particle impurity scatterings but suggests disorder-induced enhancement of the metal-insulator critical fluctuations.

As for superconductivity, T_{SC} decreases linearly with an increase in R_0 following x-ray irradiation [Fig. 3(f)], as in κ-$(ET)_2Cu(NCS)_2$ [27] and κ-$(ET)_2Cu[N(CN)_2]Br$ [28]. Although the symmetry of the superconductivity in κ-$(ET)_2X$ has not yet been fully determined, a majority of experiments support non-s-wave Cooper pairing [29]. According to the Abrikosov-Gorkov (AG) theory for the nonmagnetic impurity effect on non-s-wave superconductivity [30], the variation of T_{SC} in the small-scattering-rate limit ($1/\tau \to 0$) is described by $\ln(T_{SC}/T_{SC0}) = \psi(1/2) - \psi(1/2 + \hbar/4\pi k_B T_{SC}\tau)$, where T_{SC0} is the clean limit of T_{SC}, $\psi(x)$ is the digamma function, $\hbar$ is the Planck constant divided by 2π, and k_B is Boltzmann's constant. The relation yields $T_{SC0} - T_{SC} \simeq \pi\hbar/8k_B\tau \propto \rho_{\|0} \propto R_0$, as observed in Fig. 3(f). The observed linearity of $|dT_{SC}/dR_0| = 4$ K/Ω corresponds to $|dT_{SC}/d\rho_{\|0}| = 0.02$–$0.06$ K/$\mu\Omega$ cm. The AG theoretical value, estimated from the Fermi-surface characteristics [31] and effective mass [32], is $|dT_{SC}/d\rho_{\|0}| = 0.08$–$0.09$ K/$\mu\Omega$ cm, which is nearly in the range of the above estimate. The disorder introduced in the present experiments is so weak that it causes only a 10% reduction in T_{SC} of the non-s-wave superconductivity for $t_{irr} = 50$ h. Hence, the drastic suppression of the critical end point of the first-order Mott transition is a marked feature.

An insight into the drastic suppression of the critical end point of the first-order transition is provided by the correspondence between the Mott transition of electrons and ferromagnetic transition of Ising spins, both of which have scalar order parameters [33,34], although the critical exponents are controversial in κ-Cl; classical two-dimensional (2D) Ising values versus unconventional values possibly connected to the metal-insulator quantum criticality are under debate [35–44]. According to Harris's criterion [45], the effect of disorder is relevant when $\nu d = 2\beta + \gamma \leqslant 2$, with the correlation length exponent ν and spatial dimension d. In the 2D Ising case, in which the critical exponents (β, δ, γ) are (1/8, 15, 7/4) and thus $\nu d = 2$, disorder is marginally relevant. This may hold true even in the other case under debate since the unconventional criticality, if any, should cross over to the classical Ising criticality upon closely approaching the finite-temperature critical point [36]. According to Imry and Ma's argument [46], the 2D random-field Ising model does not show a phase transition at finite temperatures, which pertains to rapid suppression of the critical end point by introducing a weakly disordered potential, suggesting that two-dimensionality is key to the fragility of the first-order nature of the Mott transition. The finite values of T_{ep} may be due to nonzero interlayer coupling. When the first-order magnetic transition in Ising spins is

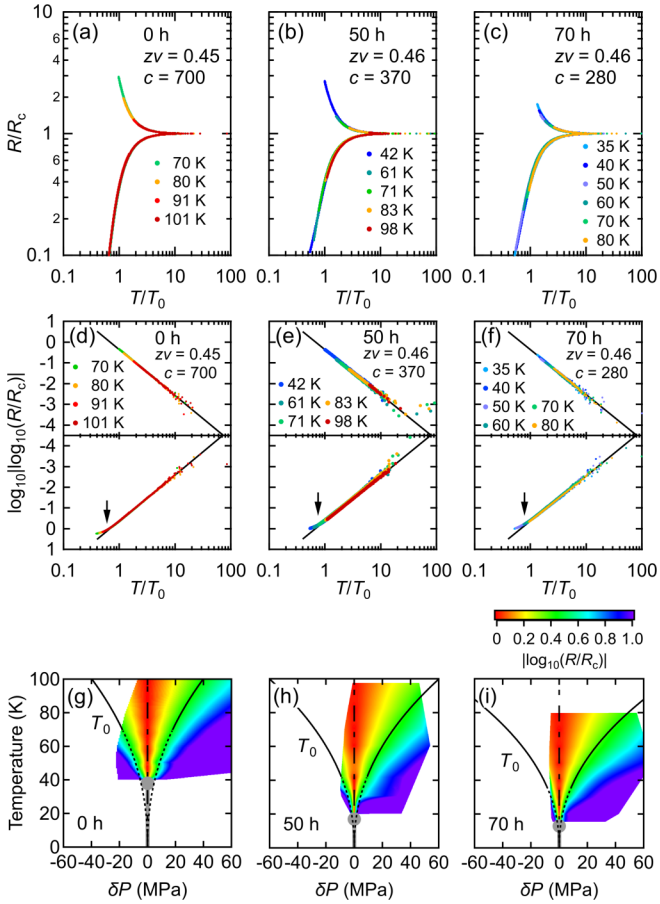

FIG. 4. (a)–(c) Quantum critical scaling of renormalized resistance R/R_c. (d)–(f) Plots of $\log_{10}|\log_{10}(R/R_c)|$ versus T/T_0. Top and bottom panels show insulating and metallic branches, respectively. Solid lines represent the quantum critical behavior $R/R_c = \exp[\pm(T/T_0)^{-1/z\nu}]$. (g)–(i) Color plots of $|\log_{10}(R/R_c)|$ in the δP-T plane. The thick gray lines and black curves represent the first-order transition lines and T_0, respectively. The point of $(\delta P, T) = (0, 0)$, the origin of the T_0 curve (indicated by a dashed curve), is a hypothetical quantum critical point.

suppressed by disorder, the Griffiths phase with spatially inhomogeneous and temporally fluctuating locally ordered domains (or droplets) emerges [47,48]. Its charge counterpart, the "electronic Griffiths phase," was theoretically proposed for the Mott transition [49] and was recently suggested by the observation of extraordinarily slow dynamics in an organic system [50]. An analogous situation likely arises in temperatures close to T_{ep}, for example, below T^*_{ep}.

Remarkably, the suppression of the critical end point of the first-order Mott transition and drop-off in the Fermi-liquid coherence temperature are followed by the prevailing of Mott quantum criticality (Fig. 4; see also the Supplemental Material [22]). Before x-ray irradiation, resistance shows quantum critical scaling well above T_{ep} [18], consistent with the prediction from the dynamical mean-field theory [17,51]; namely, renormalized resistance R/R_c follows $R/R_c = \exp[\pm(T/T_0)^{-1/z\nu}]$ (+: insulating branch, −: metallic branch), where $R_c(T)$ is the resistance on the Widom line of the Mott transition $P_{cross}(T)$, defined by peak position in $|(1/G)\partial G/\partial P|$ at a given temperature, and T_0 is the characteristic temperature defined as $T_0 = |c\delta P|^{z\nu}$, with an arbitrary constant c and pressure distance from the Widom line $\delta P = P - P_{cross}$. The same analysis for the resistance data for $t_{irr} = 50$ and 70 h found that quantum critical scaling occurred for both sets of data in intermediate temperature ranges above the reduced values of T_{ep} (Fig. 4; see also the Supplemental Material [22]). The exponent $z\nu$, a product of the dynamical and coherence length exponents, is 0.45, 0.46, and 0.46 for $t_{irr} = 0$, 50, and 70 h, respectively, which is close to the value of 0.49 that was previously determined for a pristine sample [18]. These values considerably differ from 2.0 to 2.1, which occurs in the 2D disorder-dominated metal-insulator transition in Si metal oxide–semiconductor field-effect transistors [52], suggesting that the present metal-insulator transition is interaction dominated. Note that the quantum critical region is extended to lower temperatures with increasing disorder [Figs. 4(g)–4(i)], which explains why the insulating features of resistance become less prominent with the increasing x-ray dose [Figs. 1(b) and 1(c)]. Consistently, the characteristic temperature for quantum critical scaling T_0 decreases with increasing disorder [Figs. 4(d)–4(f)]; note that because quantum critical fluctuations prevail for $T > T_0$, a decrease in T_0 indicates the extension of the quantum critical region, which means the enhancement of quantum critical fluctuations. The metallic branches deviate from the quantum critical behavior at $T^*_0 \sim 0.6T_0$, $0.75T_0$, and $0.78T_0$ for $t_{irr} = 0$, 50, and 70 h, as indicated by arrows in Figs. 4(d)–4(f), which correspond to the crossover from the high-temperature quantum critical state into the low-temperature Fermi-liquid state. The insulating branches do not reach the crossover, which would be located at negative pressures.

In a pristine crystal, the Mott localization is quantum critical at high temperatures, followed by a first-order transition below T_{ep}. As seen above, however, the first-order transition is extremely fragile against disorder; T_{ep} is reduced by more than 50% by such a weak disorder, which yields only several tens of $\mu\Omega$ cm in $\rho_{\parallel 0}$ and only a 10% reduction in T_{SC} for non-s-wave superconductivity. Thus, disorder is impactful in the first-order transition; however, the strength of the disorder itself is not significant, as seen from its effect on $\rho_{\parallel 0}$ and T_{SC}. If the energy scale of disorder is less than the thermal energy in the temperature range where the first-order transition is extinguished, then Mott quantum criticality is expected to be restored. This is suggested to be the case by the fact that the x-ray-irradiated sample fulfills the quantum critical scaling of resistance with the same $z\nu$ value as in the pristine sample. Weak disorder unveils the Mott quantum criticality hidden behind the first-order transition in two dimensions.

The behavior of interacting electrons is dominated by the energy scales of interaction, kinetics, and disorder, represented by the on-site Coulomb repulsion U, Fermi energy ϵ_F, and inverse lifetime $\hbar/\tau$, respectively. The present work targeted the region $U \sim \epsilon_F \gg \hbar/\tau$. If the system enters into a strongly disordered regime, in which the residual resistivity near the MIT reaches the Mott-Ioffe-Regel limit, the electronic Griffiths phase, whose symptom is observed near T_{ep}, can be vital, or a separate criticality may emerge, which is an interesting issue to be addressed in the future.

IV. CONCLUSIONS

To summarize, we examined the impact of weak disorder on the Mott transition and the Mott criticality in an x-ray-irradiated organic conductor, κ-Cl, by performing the resistance measurements under continuously controlled He-gas pressure. Remarkably, the critical end point of the first-order Mott transition decreases much more rapidly than the transition temperature of the disorder-sensitive non-s-wave superconductivity, highlighting the extreme fragility of the Mott critical end point to disorder. The suppression of the critical end point is accompanied by the depression of the coherence temperature of the Fermi liquid on the metallic side, which suggests that the disorder enhances the critical fluctuations of the metal-insulator transition. Concomitantly, the quantum critical scaling analysis found that the scaling held even after irradiation in intermediate temperature ranges above the decreased critical end point, consistent with the fact that the characteristic temperature for quantum critical scaling decreases. These results demonstrate that the Mott quantum critical fluctuations hidden behind the first-order transition are revealed by disorder.

ACKNOWLEDGMENTS

This work was supported by JSPS Grants-in-Aid for Scientific Research (S) (Grants No. JP25220709 and No. JP18H05225) and for Scientific Research (C) (Grant No. JP17K05532) and the Murata Scientific Foundation.

[1] J. Yi, L. Zhang, and G. S. Canright, Phys. Rev. B **49**, 15920 (1994).
[2] M. Ulmke and R. T. Scalettar, Phys. Rev. B **55**, 4149 (1997).
[3] H. Shinaoka and M. Imada, J. Phys. Soc. Jpn. **78**, 094708 (2009); Phys. Rev. Lett. **102**, 016404 (2009).
[4] S. Chiesa, P. B. Chakraborty, W. E. Pickett, and R. T. Scalettar, Phys. Rev. Lett. **101**, 086401 (2008).
[5] D. Heidarian and N. Trivedi, Phys. Rev. Lett. **93**, 126401 (2004).
[6] M. E. Pezzoli and F. Becca, Phys. Rev. B **81**, 075106 (2010).
[7] D. Tanasković, V. Dobrosavljević, E. Abrahams, and G. Kotliar, Phys. Rev. Lett. **91**, 066603 (2003).
[8] M. C. O. Aguiar, V. Dobrosavljević, E. Abrahams, and G. Kotliar, Phys. Rev. Lett. **102**, 156402 (2009).
[9] M. C. O. Aguiar and V. Dobrosavljević, Phys. Rev. Lett. **110**, 066401 (2013).
[10] H. Bragança, M. C. O. Aguiar, J. Vučičević, D. Tanasković, and V. Dobrosavljević, Phys. Rev. B **92**, 125143 (2015).
[11] K. Byczuk, W. Hofstetter, and D. Vollhardt, Phys. Rev. Lett. **94**, 056404 (2005); **102**, 146403 (2009).
[12] H. Lee, H. O. Jeschke, and R. Valentí, Phys. Rev. B **93**, 224203 (2016).
[13] K. Kanoda and R. Kato, Annu. Rev. Condens. Matter Phys. **2**, 167 (2011).
[14] K. Miyagawa, A. Kawamoto, Y. Nakazawa, and K. Kanoda, Phys. Rev. Lett. **75**, 1174 (1995).
[15] F. Kagawa, T. Itou, K. Miyagawa, and K. Kanoda, Phys. Rev. B **69**, 064511 (2004).
[16] P. Limelette, P. Wzietek, S. Florens, A. Georges, T. A. Costi, C. Pasquier, D. Jérome, C. Mézière, and P. Batail, Phys. Rev. Lett. **91**, 016401 (2003).
[17] H. Terletska, J. Vučičević, D. Tanasković, and V. Dobrosavljević, Phys. Rev. Lett. **107**, 026401 (2011).
[18] T. Furukawa, K. Miyagawa, H. Taniguchi, R. Kato, and K. Kanoda, Nat. Phys. **11**, 221 (2015).
[19] T. Sasaki, Crystals **2**, 374 (2015).
[20] N. Yoneyama, T. Sasaki, N. Kobayashi, K. Furukawa, and T. Nakamura, Phys. B (Amsterdam, Neth.) **405**, S244 (2010).
[21] L. Kang, K. Akagi, K. Hayashi, and T. Sasaki, Phys. Rev. B **95**, 214106 (2017).
[22] See Supplemental Material at http://link.aps.org/supplemental/10.1103/PhysRevB.99.245139 for experimental details and supporting results.
[23] E. Gati, U. Tutsch, A. Naji, M. Garst, S. Köhler, H. Schubert, T. Sasaki, and M. Lang, Crystals **8**, 38 (2018).
[24] H. Ito, M. Kubota, Y. V. Sushko, N. Kojima, G. Saito, and T. Ishiguro, Synth. Met. **70**, 925 (1995).
[25] H. Ito, T. Ishiguro, M. Kubota, and G. Saito, J. Phys. Soc. Jpn. **65**, 2987 (1996).
[26] A. J. Schultz, U. Geiser, H. H. Wang, J. M. Williams, L. W. Finger, and R. M. Hazen, Phys. C (Amsterdam, Neth.) **208**, 277 (1993).
[27] J. G. Analytis, A. Ardavan, S. J. Blundell, R. L. Owen, E. F. Garman, C. Jeynes, and B. J. Powell, Phys. Rev. Lett. **96**, 177002 (2006).
[28] K. Sano, T. Sasaki, N. Yoneyama, and N. Kobayashi, Phys. B (Amsterdam, Neth.) **405**, S279 (2010).
[29] K. Miyagawa, K. Kanoda, and A. Kawamoto, Chem. Rev. **104**, 5635 (2004).
[30] B. J. Powell and R. H. McKenzie, Phys. Rev. B **69**, 024519 (2004).
[31] Y. Yamauchi, M. V. Kartsovnik, T. Ishiguro, M. Kubota, and G. Saito, J. Phys. Soc. Jpn. **65**, 354 (1996).
[32] K. Oshima, T. Mori, H. Inokuchi, H. Urayama, H. Yamochi, and G. Saito, Phys. Rev. B **38**, 938(R) (1988).
[33] C. Castellani, C. Di Castro, D. Feinberg, and J. Ranninger, Phys. Rev. Lett. **43**, 1957 (1979).
[34] G. Kotliar, E. Lange, and M. J. Rozenberg, Phys. Rev. Lett. **84**, 5180 (2000).
[35] M. de Souza, A. Brühl, C. Strack, B. Wolf, D. Schweitzer, and M. Lang, Phys. Rev. Lett. **99**, 037003 (2007).
[36] T. Misawa and M. Imada, Phys. Rev. B **75**, 115121 (2007).
[37] S. Papanikolaou, R. M. Fernandes, E. Fradkin, P. W. Phillips, J. Schmalian, and R. Sknepnek, Phys. Rev. Lett. **100**, 026408 (2008).
[38] M. Sentef, P. Werner, E. Gull, and A. P. Kampf, Phys. Rev. B **84**, 165133 (2011).
[39] F. Kagawa, K. Miyagawa, and K. Kanoda, Nature (London) **436**, 524 (2005); Nat. Phys. **5**, 880 (2009).

[40] M. Abdel-Jawad, R. Kato, I. Watanabe, N. Tajima, and Y. Ishii, Phys. Rev. Lett. **114**, 106401 (2015).
[41] L. Bartosch, M. de Souza, and M. Lang, Phys. Rev. Lett. **104**, 245701 (2010).
[42] M. Zacharias, L. Bartosch, and M. Garst, Phys. Rev. Lett. **109**, 176401 (2012).
[43] M. Zacharias, A. Rosch, and M. Garst, Eur. Phys. J. Spec. Top. **224**, 1021 (2015).
[44] E. Gati, M. Garst, R. S. Manna, U. Tutsch, B. Wolf, L. Bartosch, H. Schubert, T. Sasaki, J. A. Schlueter, and M. Lang, Sci. Adv. **2**, e1601646 (2016).
[45] A. B. Harris, J. Phys. C **7**, 1671 (1974).
[46] Y. Imry and S. Ma, Phys. Rev. Lett. **35**, 1399 (1975).
[47] O. Motrunich, K. Damle, and D. A. Huse, Phys. Rev. B **63**, 134424 (2001).
[48] T. Vojta, J. Low. Temp. Phys. **161**, 299 (2010).
[49] E. C. Andrade, E. Miranda, and V. Dobrosavljević, Phys. Rev. Lett. **102**, 206403 (2009).
[50] T. Itou, E. Watanabe, S. Maegawa, A. Tajima, N. Tajima, K. Kubo, R. Kato, and K. Kanoda, Sci. Adv. **3**, e1601594 (2017).
[51] J. Vučičević, H. Terletska, D. Tanasković, and V. Dobrosavljević, Phys. Rev. B **88**, 075143 (2013).
[52] P. V. Lin and D. Popović, Phys. Rev. Lett. **114**, 166401 (2015).